JOURNAL OF GEOPHYSICAL RESEARCH, VOL. 110, C09021, doi:10.1029/2004JC002834, 2005

Energy and momentum dissipation through wave breaking

Shuwen Zhang and Yeli Yuan

Key Laboratory of Marine Science and Numerical Modeling, First Institute of Oceanography, State Oceanic Administration, Qingdao, China

Received 2 December 2004; revised 11 May 2005; accepted 27 May 2005; published 28 September 2005.

[1] Wave breaking plays an important role in air-sea interaction. Laboratory and field measurements suggest that the wave field dissipation can be significantly enhanced by wave breaking and acts as a source of energy for generating current and entraining air against the effect of buoyancy forces. In the present study, a breaking wave model is formulated by taking the acceleration threshold value of $-g/2$ as breaking criterion, and the statistics of breaking waves, such as breaking wave coverage per unit time, and the volume of breaking water per unit area of wave surface per unit time are estimated. Statistical models are also developed to assess energy and momentum dissipation through wave breaking. It is found that the energy and momentum dissipation rates decay as k^{-3} and $k^{-2.5}$, respectively. The energy loss is mainly due to wave components at frequencies higher than the spectral peak frequency. Though energy loss due to wave components at frequencies lower than the spectral peak frequency is found, these wave components do not significantly lose energy after the breaking. The energy loss, when expressed as phase speed c_b of breaking waves, is mainly in the range $0.20\ c_p < c_b < 0.90\ c_p$, where c_p is the dominant wave phase speed, and the energy dissipation rate falls off rapidly toward shorter scales. This offers no support for the hypothesis of a "Kolmogorov cascade" in wind-generated waves analogous to that in turbulence, with energy input from the wind at large scales and dissipation from the waves at the smallest scales. It is also demonstrated that, compared with empirical formula results, our model of energy (or momentum) dissipation rate lies between those models that estimate by empirical formula the rate of energy (or momentum) loss from a breaker with proportional coefficients 0.0085 and 0.0007. In addition, the peak frequency of our model energy (or momentum) dissipation rate downshifts to the lower-frequency band as wind speed increases, whereas the peak of the empirical formula remains at the same frequency.

Citation: Zhang, S., and Y. Yuan (2005), Energy and momentum dissipation through wave breaking, *J. Geophys. Res.*, *110*, C09021, doi:10.1029/2004JC002834.

1. Introduction

[2] The dynamical coupling between the atmosphere and the ocean is mediated by the surface waves. The development of the wave field depends on wind energy input, wave-wave interaction, wave-current interaction, and wave field dissipation by breaking. Breaking waves, being the visual manifestation of the air-sea interaction, enhance the wave dissipation, which is believed to generate surface current and eddies and entrain air against the effect of buoyancy forces [*Mitsuyasu*, 1985; *Melville and Rapp*, 1985; *Yuan et al.*, 1990; *Lamarre and Melville*, 1991; *Agrawal et al.*, 1992; *Thorpe*, 1993; *Gemmrich et al.*, 1994; *Melville*, 1994; *Terray et al.*, 1996; *Phillips et al.*, 2001; *Melville and Matusov*, 2002; *Deane and Stokes*, 2002]. Breaking waves also enhance the air-sea exchange of mass, heat, and gases by the local increase in turbulence associated with breaking and by entrainment of air that breaks up into bubbles [*Monahan and Spillane*, 1984; *Csanady*, 1990; *Thorpe*, 1992, 1995; *Melville*, 1996; *Jessup et al.*, 1997; *Erickson et al.*, 1999; *Zappa et al.*, 2001; *Zhang and Yuan*, 2004; *Graham et al.*, 2004; *Graham*, 2004], which has a profound effect on climate and weather.

[3] Using the output data of National Ocean and Atmospheric Administration/National Center for Environmental Prediction (NOAA/NCEP), *Wang and Huang* [2004a] concluded that a large fraction of the energy transported from wind to water is absorbed by the surface waves, and only a small fraction of winds energy is input to the Ekman layer [*Wang and Huang*, 2004b]. This gives direct evidence to show that surface waves play a dominant role in the energy transfer from wind to the ocean. Laboratory measurements made by *Melville and Rapp* [1985] suggested that up to 40% of the total wave energy may be lost through breaking. However, the energy and momentum dissipation through wave breaking remains a problem because field observation is extremely difficult. There is no complete agreement on the adequacy of the models for the wave dissipation through breaking. In this paper, we mainly

0148-0227/05/2004JC002834$09.00

discuss the energy and momentum dissipation by wave breaking based on a breaking wave model.

2. Breaking Wave Model and its Statistics

2.1. Breaking Wave Model and its Spectrum

[4] Waves break on a variety of scales. Small-scale ripples or capillary waves formed on the crest or leading face of steep gravity waves can cause small-scale breaking [*Banner and Phillips*, 1974; *Jessup et al.*, 1997; *Zappa et al.*, 2001]. The more familiar breaking occurs on a large scale, with spilling or plunging, entraining air to create dense plumes of bubbles that can extend 0.5 m or more below the surface [*Lamarre and Melville*, 1992; *Farmer and Gemmrich*, 1996; *Deane and Stokes*, 2002].

[5] *Longuet-Higgins* [1963] examined the breaking mechanism of Stokes waves and pointed out that a breaker only occurs at the wave crest when the downward acceleration reaches $-g/2$, where g is the acceleration of gravity. Laboratory measurements by *Lou* [1997] and field observations by *Snyder et al.* [1983] also supported a breaking criterion of $-g/2$. In contrast, other investigations of random, deepwater wave fields have suggested acceleration threshold values of less than $g/2$ [*Holthuijsen and Herbers*, 1986; *Dawson et al.*, 1993]. The discrepancy between different observations may be attributed to differences in Eulerian and Lagrangian observational methods, as well as to the influence of multiple-frequency superposition and directionality on real crest acceleration [*Nepf et al.*, 1998]. Although it remains for further experiments to provide a definitive answer to this issue, some insight can be obtained by examining the experimental results of *Lou* [1997]. *Lou* [1997] measured the downward accelerations at three different cases: (1) before breaking (at the moment very near to breaking), (2) at breaking (fluid appears to break out of the surface and white water falls down the front face of wave), and (3) after breaking (whitecaps occur at the surface). As reported by *Lou* [1997], among 10 different breaking wave trains the experimental results supported a breaking criterion of $-g/2$ in case 1. However, in both cases 2 and 3 the downward accelerations are less than $g/2$. Laboratory experiments of *Lou* [1997] also implied that the breaking acceleration threshold should be measured at the moment very near to breaking rather than after breaking when whitecaps occur at the surface. In the present study, taking the limited condition $\partial^2\zeta/\partial t^2$ (hereinafter $\ddot{\zeta}$) $\leq -g/2$ as the criterion of breaking acceleration threshold, the breaking waves model can be proposed as

$$\zeta_{\mathrm{B}} = \zeta\left\{\frac{g/2}{|\ddot{\zeta}|}H\left(-\frac{g}{2}-\ddot{\zeta}\right)+H\left(\frac{g}{2}+\ddot{\zeta}\right)\right\}, \qquad (1)$$

where ζ denotes the prebreaking surface elevation, ζ_B is the surface elevation after breaking, $\ddot{\zeta}$ is the Eulerian acceleration, and $H(\ )$ denotes the Heaviside unit function. Model (1) implies that at wave breaking, ζ_B is decreased locally from ζ by a factor of $0.5g/|\ddot{\zeta}|$. A comparison will be given in section 3 by using different breaking acceleration thresholds ($0.5g$ and $0.4g$) to test how sensitive the present model predictions are to the breaking acceleration threshold conditions.

[6] The wave spectrum after breaking can be obtained by calculating the Fourier transform of the correlation function $E\{\zeta_B(x, t_1)\zeta_B(x, t_2)\}$ as

$$S_B(\omega) = \left[M - \left(\frac{\omega}{\omega_B}\right)^2 N\right]^2 S(\omega), \qquad (2)$$

where E{ } represents the ensemble average, $S(\omega)$ and $S_B(\omega)$ are the one-dimensional frequency spectrum of ζ and ζ_{B}, respectively, and ω is the frequency [*Hua and Yuan*, 1991]. Letting μ_i represent the ith-order moment of $S(\omega)$, $\omega_B = (\mu_4/\mu_2)^{1/2}$, M and N can be expressed as follows:

$$M \approx 1 - \frac{1}{\sqrt{2\pi\sigma^3}}\exp\left(-\frac{\sigma^2}{2}\right), \qquad (3)$$

$$N = \frac{1}{\sqrt{2\pi\sigma}}\left(1-\frac{2}{\sigma^2}\right)\exp\left(-\frac{\sigma^2}{2}\right), \qquad (4)$$

where $\sigma = 1/\sqrt{2\Phi_B}$ and Φ_B is the breaking wave coverage per unit time. The filter function $[M - (\omega/\omega_B)^2\ N]^2$ in (2) describes the variation of wave spectrum during wave breaking.

[7] In the present study, we consider a finite depth of water and take the wave age parameter as 2.0. The dispersion relation and phase speed of sea waves are defined by

$$\omega^2 = \left(gk + \frac{\gamma k^3}{\rho_w}\right)\tanh(kd), \qquad (5)$$

$$c = \sqrt{\left(\frac{g}{k}+\frac{\gamma k}{\rho_w}\right)\tanh(kd)}, \qquad (6)$$

where γ is the surface tension, d is the water depth, and ρ_w is the water density. The wave number spectrum $S_B(k)$ can be obtained by converting frequency spectrum $S_B(\omega)$ via the adopted dispersion relationship for long and short waves. Additionally, the total energy should be preserved after conversion. The one-dimensional wave number spectrum $S(k)$ adopted in this study is the one proposed by *Elfouhaily et al.* [1997] expressed as a sum of two spectra regimes

$$S(k) = k^{-3}(B_l(k) + B_h(k)), \qquad (7)$$

where subscripts l and h indicate low and high frequencies, respectively, and B stands for the curvature spectrum. The long-wave spectrum, $S(k) = k^{-3}\ B_l(k)$, depends on the dimensionless inverse wave age parameter U_{10}/c_p, where U_{10} is the wind speed at a height of 10 m above the sea surface. The short-wave spectrum, $k^{-3}\ B_h(k)$, depends on the dimensionless parameter (u_*/c_m), where u_* is the friction velocity at the sea surface, c_m is the minimum phase speed (c_m = 0.23 m s^{-1}) at the wave number associated with a supposed gravity-capillary peak in the curvature spectrum. It should be emphasized that for some wave spectra, including the theoretical and experimental spectra, the fourth-order spectral moment does not exist. The usual means of handling such problems involving fourth-order

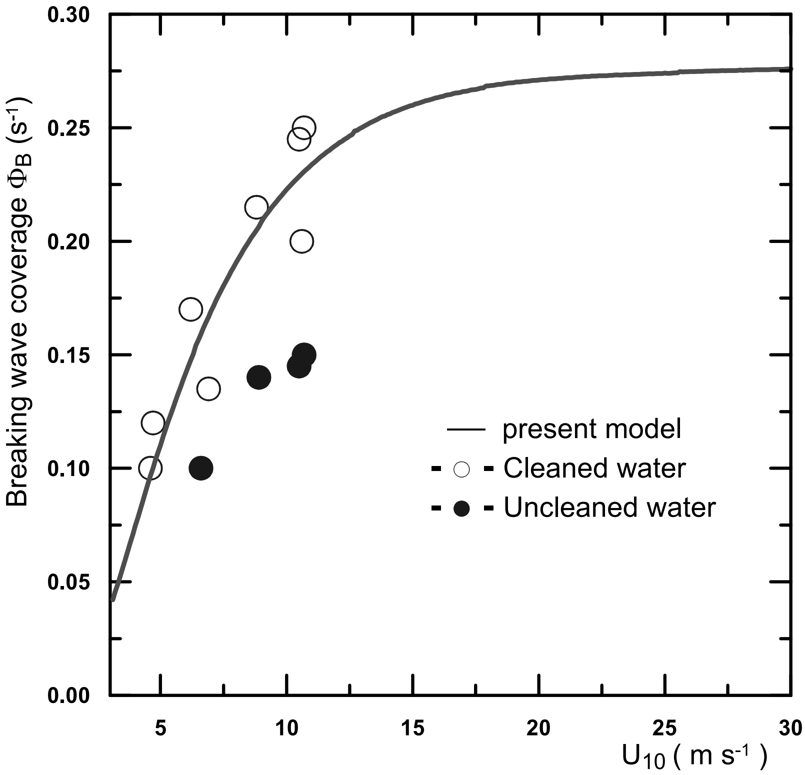

Figure 1. Breaking wave coverage Φ_B (s^{-1}) versus wind speed of U_{10}. Solid line presents our model results; open circles (cleaned water surface) and solid circles (surfactant-influenced surface) represent the data measured by *Zappa et al.* [2001] in a wind-wave tank using passive IR imagery technique for wind speeds from 4.6 to 10.7 m s^{-1}.

spectral moment include the use of a frequency cutoff in which the upper limit is replaced with some finite value. However, such a treatment has serious theoretical deficiencies and leads to inconsistent quantitative results. The wave number spectrum proposed by *Elfouhaily et al.* [1997] has the ability to properly describe diverse fetch conditions and to provide agreement with in situ observations of *Cox and Munk* [1954], *Jähne and Riemer* [1990], and *Hara et al.* [1994] data in the high wave number regime. Furthermore, the fourth-order spectral moment can be calculated without the need to cut off the higher-frequency components.

2.2. Statistics of Breaking Waves

[8] According to *Yuan et al.* [1990] the breaking wave coverage Φ_B per unit time and the volume of breaking water V_B per unit time and per unit area of wave surface can be obtained by

$$\Phi_B = \frac{1}{T}\int_0^T \left[\frac{1}{S}\iint_S H\left(-g/2 - d^2\zeta/dt^2\right)dS\right]dt = \frac{1}{4\sqrt{2}\pi}\left(\frac{\mu_4}{\mu_2}\right)^{1/2}\exp\left(-\frac{g^2}{8\mu_4}\right), \quad (8)$$

$$V_B = \frac{1}{T}\int_0^T \left[\frac{1}{S}\iint_S (\zeta - \zeta_B)dS\right]dt \approx \frac{\mu_0^{1/2}\mu_4^{3/2}}{2\pi^{3/2}g^2\mu_2^{1/2}}\exp\left(-\frac{g^2}{8\mu_4}\right), \quad (9)$$

where T and S denote the time interval and area of wave surface, respectively. It should be noted that the wave-related parameter Φ_B is the same as the breaking rate and V_B denotes the volume within which bubbles are produced by breaking waves. The volume of breaking water, physically, relates to breaking wave coverage by $V_B = \Delta h \Phi_B$, where Δh is the vertical thickness of the breaking water. A brief justification of equations (8) and (9) is supplemented in Appendix A.

[9] As a first approximation the breaking wave coverage is expected to closely follow wind speed. However, our model results indicate that the breaking wave coverage is not linearly correlated with the wind speed. As shown in Figure 1, the breaking wave coverage estimated by our model (solid line) increases from 0.05 to 0.27 s^{-1}, as wind speed ranges from 3.0 to 30 m s^{-1}; this is in good agreement with the laboratory measurements of fractional surface area covered by surface renewal generated through wave breaking, as reported by *Zappa et al.* [2001] for wind speeds from 4.6 to 10.7 m s^{-1}.

[10] Its worth noting that though our model results fit with the laboratory measurements of fractional surface area covered by surface renewal generated because of wave breaking, they are much higher than the breaking rates measured in the open sea. This may be partly attributed to the observation techniques of breaking rate. The available techniques used in the open sea focus on wave breaking at larger scales; the presence of small-scale breakers is largely ignored. To our knowledge, smaller breakers occur much more frequently, and thus their overall contribution to the breaking rate should not be ignored.

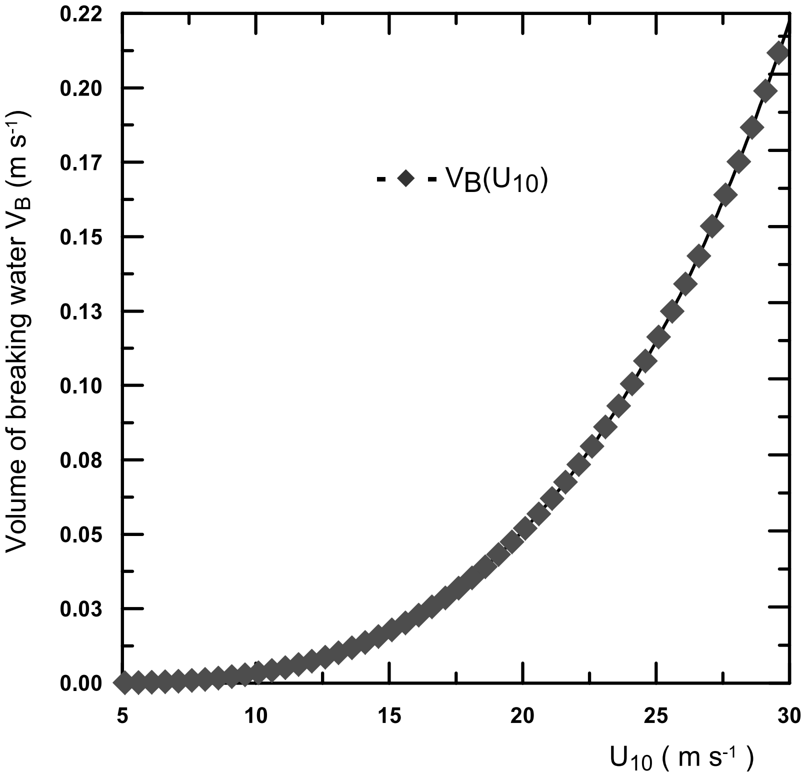

Figure 2. Volume of breaking water V_B (m s^{-1}) versus wind speed of U_{10}. Diamonds indicate present model results.

[11] The volume of breaking water is believed to be an important wave-related parameter correlated with the bubble plume generation and the transfer of momentum fluxes from the wave field to the current. Modeling by *Zhang and Yuan* [2004] suggested that the average total volume of bubbles per unit time and per unit area of wave surface is proportional to the volume of breaking water. At active wave breaking a jet of water with speed of about c is ejected forward with momentum flux per unit length of wave crest $\rho_w c^2 \Delta h/2$, where c is the wave phase velocity. Figure 2 shows the volume of breaking water V_B per unit time and per unit area of wave surface versus the wind speed. It can be seen from Figure 2 that the volume of breaking water V_B increases significantly from 0 to 0.22 m s^{-1}, as wind speed ranges from 5.0 to 30 m s^{-1}.

3. Wave Energy Loss by Wave Breaking

[12] It is of greater dynamical interest and challenge to estimate the distribution of wave energy dissipation through wave breaking. The difference between energy spectra of wave components before and after a breaker can accurately reveal the energy dissipation as a function of frequency. Figure 3 shows comparison between energy spectra of wave components before and after a breaker at wind speed of 15 m s^{-1}. It is indicated that the major energy loss occurs at frequencies higher than the peak frequency. Though energy loss due to wave components at frequencies lower than the peak frequency is found, these wave components do not significantly lose energy after breaking. These findings are similar to the observations of *Rapp and Melville* [1990], *Kway et al.* [1998], and *Meza et al.* [2000].

[13] Laboratory measurements [*Duncan*, 1981] indicated that the distribution of energy loss rate is proportional to $\rho_w g^{-1} c^5$, with a constant of $b = 0.03$. In a careful review, *Melville* [1994] inferred that in transient breaker b = (3 to 16) $\times$ 10^{-3}. Long-range radar measurements [*Phillips et al.*, 2001] suggested that wave energy dissipation by breaking is significant at large scales, and the proportional coefficient should be b = (7 to 13) $\times$ 10^{-4}. In a well-developed sea, observations made by *Melville and Matusov* [2002] concluded that wave field dissipation is proportional to U_{10}^3 and dominated by intermediate-scale waves. Because of the uncertainty of the proportional coefficient used in the empirical formula of wave field dissipation, we calculated the energy of prebreaking wave in terms of the one-dimensional wave number spectrum in a general form as [*Kinsman*, 1965]

$$e_b(k) = \frac{1}{2}\rho_w g S(k). \tag{10}$$

The wave energy after breaking can be similarly given by

$$e_a(k) = \frac{1}{2}\rho_w g S_B(k). \tag{11}$$

Consequently, the distribution of wave energy loss, $\varepsilon_{ed}(k)$, is then expressed as

$$\varepsilon_{ed}(k) = e_b(k) - e_a(k). \tag{12}$$

[14] Wave energy is dissipated, roughly, over the time taken for the wave to collapse [*Shaw*, 2003]. As measured

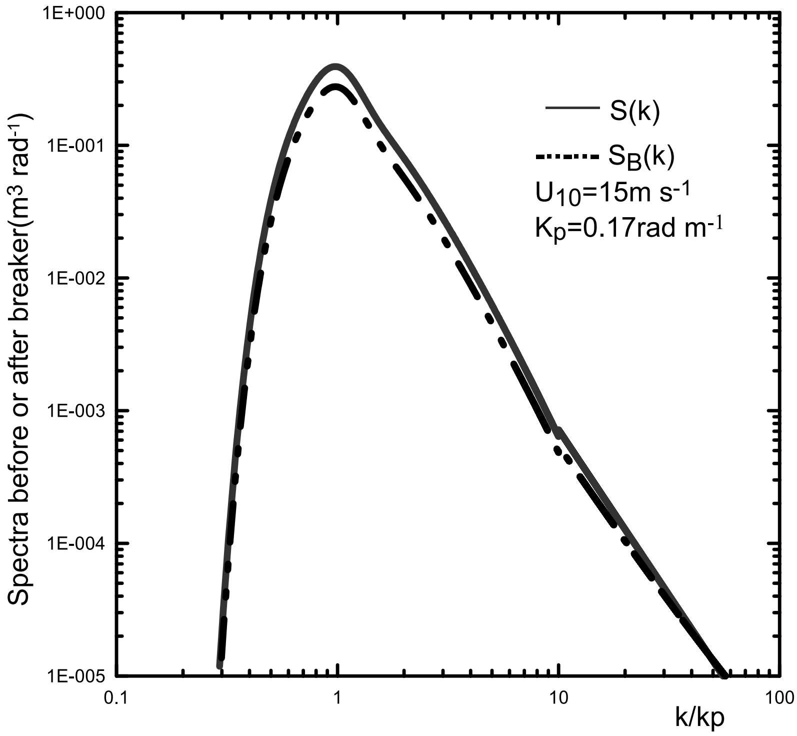

Figure 3. Comparison between wave spectra before (solid line) and after (dash-dotted line) a breaker at wind speed of 15 m s^{-1}. The spectral peak wave number k_p = 0.17 rad m^{-1}.

by *Deane and Stokes* [2002], the active wave breaking mainly consist of two processes: (1) The overturning wave crest has struck the wave face before the cavity of air trapped between the breaking water and wave face has fragmented. (2) About 1s later, a shear flow on the wave face has formed, and a layer of air trapped between the spreading jet and wave face is observed to form and split into filaments and bubbles. Therefore it is reasonable to assume that in the first process, wave energy loss at surface has almost completely ceased and acts as a source of energy

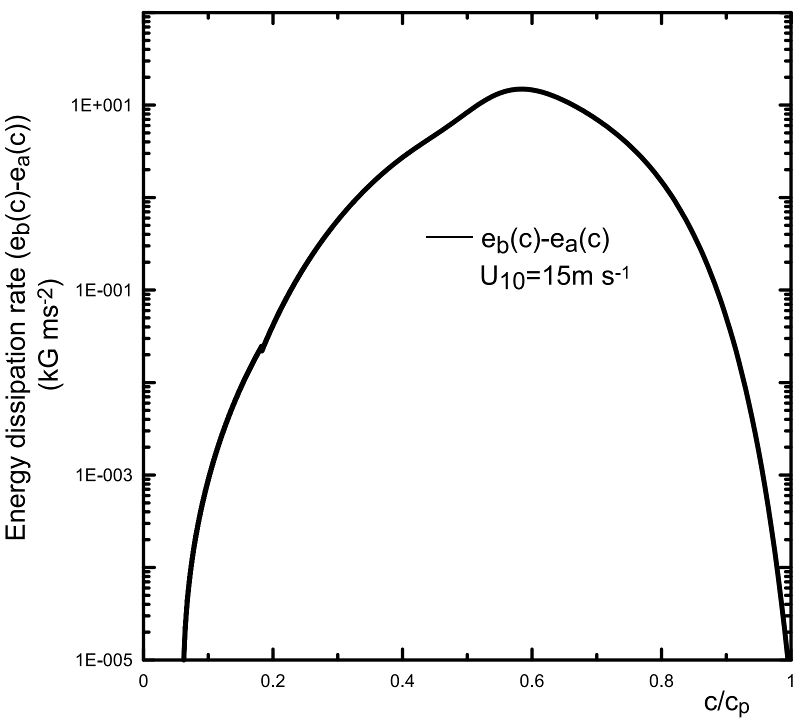

Figure 4. Energy dissipation rate versus the normalized wave phase velocity at wind speed of 15 m s^{-1}.

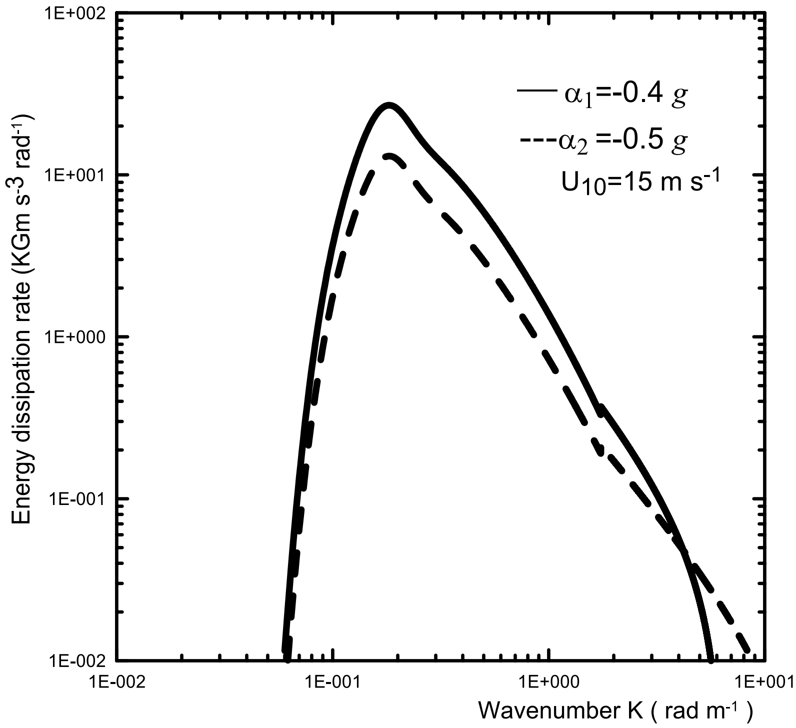

Figure 5. Comparison between our model of energy dissipation rates by using different acceleration thresholds at wind speed of 15 m s^{-1}. Solid line is for the acceleration threshold of $-0.4g$, and dashed line is for the acceleration threshold of $-0.5g$.

for generating surface current and forming a violent turbulence in breaking zone, which results in the bubble plume [*Lamarre and Melville*, 1991]. *Wu* [1992] also reported that breaking occurs at the wave crest and typically covers a few tenths of a wavelength. This implies that breaking crest will pass a stationary point in about 1s. As a consequence, the breaking energy loss rate is assumed to be proportional to the difference of wave energy levels $[e_b(k) - e_a(k)]$ throughout this article.

[15] We have shown the trend of energy loss against the normalized phase velocity. Figure 4 shows that breaking waves exist over a wide range of scales, most of them being significantly shorter than the dominant wave. The energy loss, when expressed as phase speed c_b of breaking waves, is mainly in the range $0.20\ c_p < c_b < 0.90\ c_p$. To a large extent, this is the same range as that of the dissipation scale reported by the laboratory and field observations [*Ding and Farmer*, 1994; *Smith et al.*, 1996; *Gemmrich and Farmer*, 1999; *Phillips et al.*, 2001; *Meza et al.*, 2000]. In addition, it is also implied that at the smaller values of c, the dissipation rate falls off rapidly. This is consistent with the field observations by *Melville and Matusov* [2002], which were taken under a well-developed wave condition, and offers no support for the hypothesis of a "Kolmogorov cascade" [*Kitaigorodskii*, 1992; *Zakharoff*, 1992] in wind-generated waves analogous to that in turbulence, where energy input is from the wind at large scales and dissipation is from the waves at the smallest scales, as first commented by *Phillips et al.* [2001].

[16] In order to test how sensitive the present model predictions are to the breaking acceleration threshold conditions, we have estimated the energy dissipation rates by using breaking acceleration thresholds $-0.5g$ and $-0.4g$. Figure 5 illustrates the prediction of our model about the choice of acceleration threshold. As shown, significant differences exist between those estimated with breaking acceleration thresholds $-0.5g$ and $-0.4g$, especially at frequencies higher than the peak frequency. In other words, our model prediction is sensitive to the choice of acceleration threshold. When the breaking acceleration threshold is taken as $-0.4g$, more wave energy is dissipated by breaking than that in the case of $-0.5g$.

[17] The total energy dissipation by breaking can be obtained by integrating equation (12) from $k_1 = 0.01$ to $k_2 = 370$ rad m^{-1}, then we have

$$E_b - E_a = \int_{k_1}^{k_2} \varepsilon_{ed}(k)dk, \tag{13}$$

where k_1 and k_2 correspond to the long gravity wave and the Ku-band radar backscatter measurements of gravity-capillary waves, respectively. By integrating over corresponding wave number ranges the total energy dissipation $(E_b - E_a)$ versus U_{10} is shown in Figure 6. Figure 6 illustrates that the total energy dissipation is closely proportional to U_{10}^3 as wind speed $U_{10} > 7$ m s^{-1}, which is consistent with the field observations made by *Melville and Matusov* [2002] under a well-developed wave condition.

[18] The empirical formula of energy dissipation rate by breaking with respect to the wave phase speed is given by

$$\varepsilon_{Energy} = b\rho_w g^{-1} c^5 \Lambda(c), \tag{14}$$

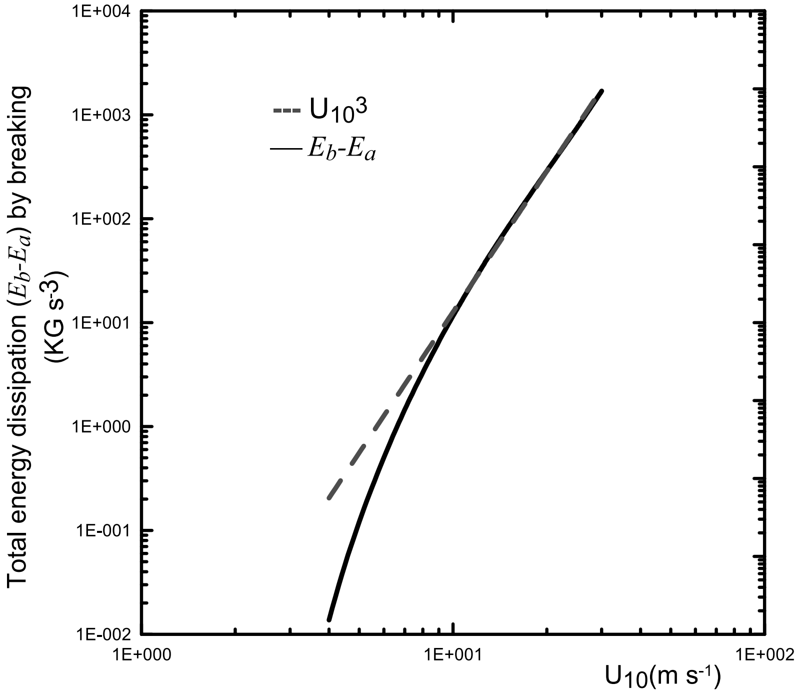

Figure 6. Total energy dissipation ($E_b - E_a$) through wave breaking versus wind speed of U_{10}. Solid line is for the model result, and dashed line is for the values of U_{10}^3. See color version of this figure in the HTML.

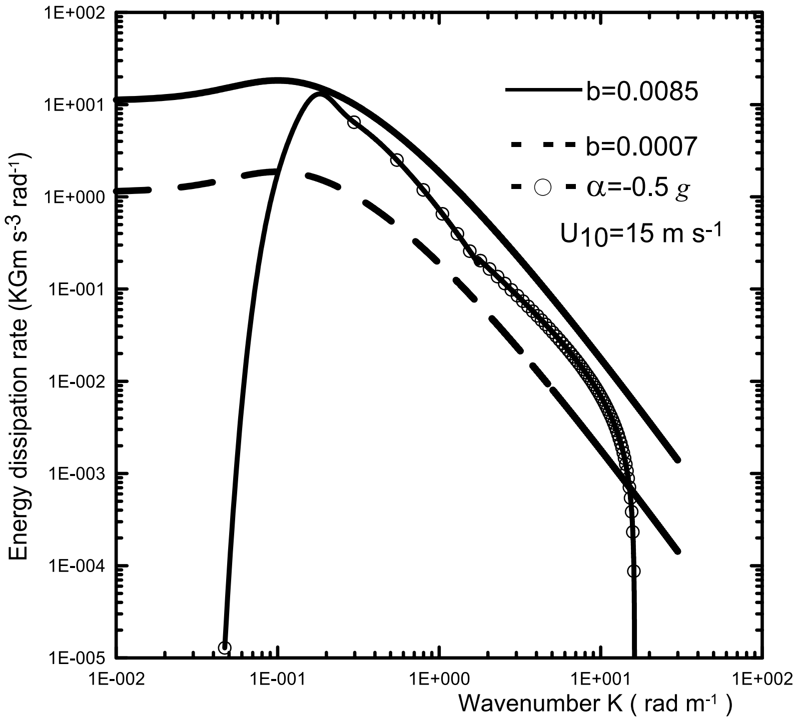

Figure 7. A comparison of energy dissipation rates between our model and those estimated by the empirical formula. Open circle is for our model result; solid line is for the empirical results with a proportional coefficient of 0.0085 suggested by *Melville and Matusov* [2002]; and dashed line is for empirical results with a proportional coefficient of 0.0007 reported by *Phillips et al.* [2001].

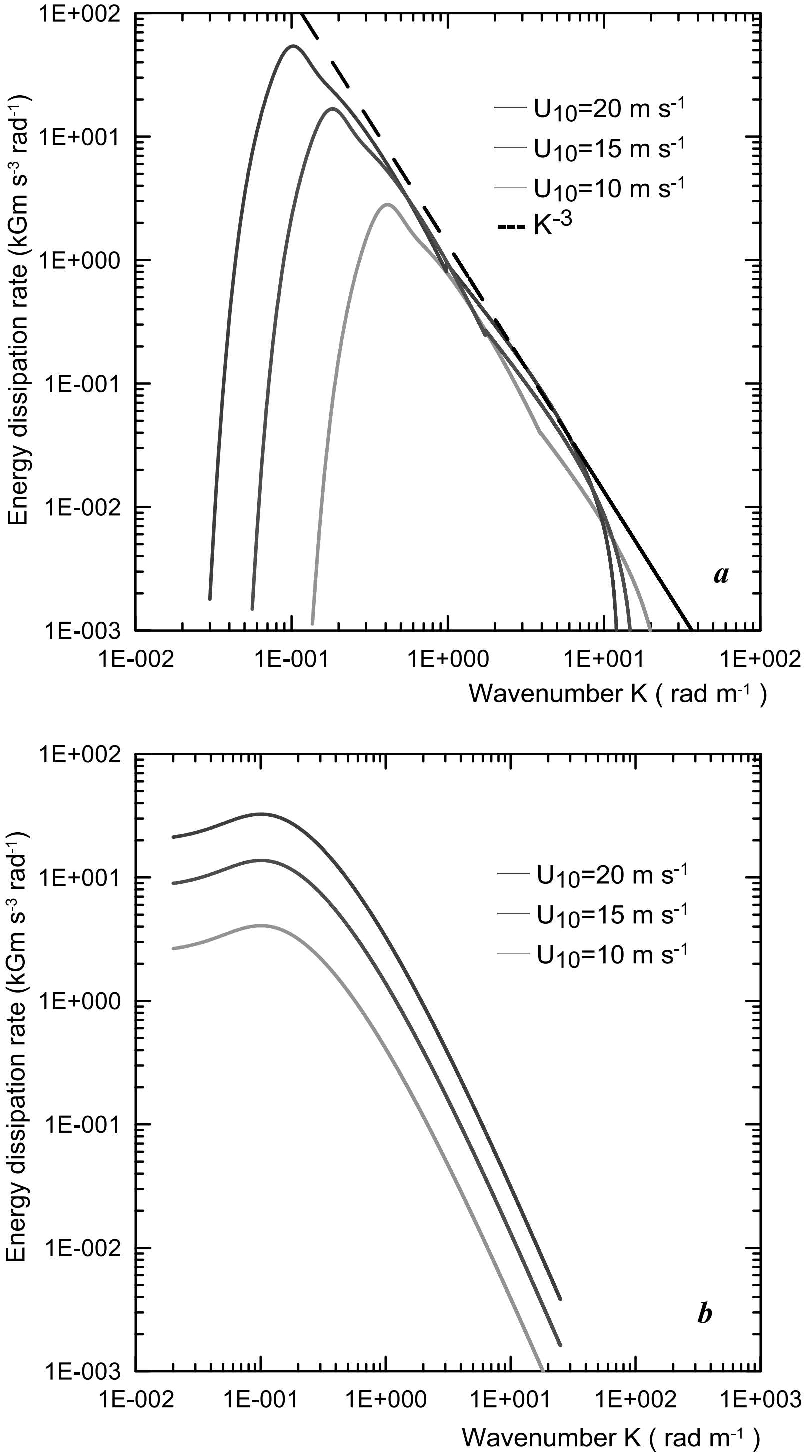

Figure 8. Energy dissipation rates estimated for wind speeds of 10, 15, and 20 m s^{-1}. (a) Model results. (b) Empirical results calculated by using equation (14) with a proportional coefficient of 0.006. See color version of this figure in the HTML.

where $\Lambda(c)dc$ is the average length of breaking crests per unit area of ocean surface traveling at velocity in the range (c, c + dc), introduced by *Phillips* [1985] as a statistical description of breaking waves. In a well-developed sea, *Melville and Matusov* [2002] had made measurements in which, when weighted by U_{10}^{-3}, $\Lambda(c)$ has the following form

$$\Lambda(c) = 3.3 \times 10^{-4} \exp(-0.64c). \tag{15}$$

Melville and Matusov [2002] also indicated that most of the wave dissipation occurs around the frequency of the characteristic breaking waves, and its phase velocity c is approximately 80% of the characteristic linear phase speed of the wave.

[19] As mentioned earlier, there was a large uncertainty in determining the proportional coefficient b supported by different observations. In the present study, we use the

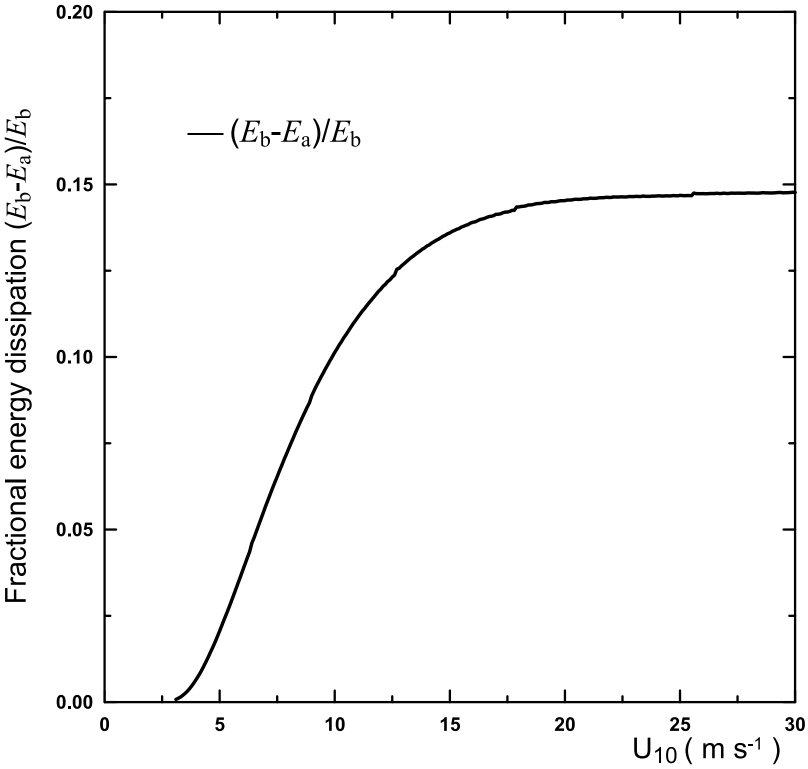

Figure 9. Fractional energy dissipation $(E_b - E_a)/E_b$ versus wind speed of U_{10}.

proportional coefficient b of 0.0085 suggested by *Melville and Matusov* [2002] and b of 0.0007 reported by *Phillips et al.* [2001]. The comparison between our model of energy dissipation rate and those estimated by empirical formula (14), at wind speed of 15 m s^{-1}, is shown in Figure 7. Our model of energy dissipation rate lies between those estimated by empirical formula with proportional coefficients 0.0085 and 0.0007. As shown in Figures 8a and 8b, on the other hand, though the peak energy dissipation rate of our model is nearly the same in magnitude with that estimated by empirical formula with a proportional coefficient of 0.006 at wind speed of 10, 15 and 20 m s^{-1}, respectively, the peak frequency of our model downshifts to the lower-frequency band as wind speed increases, whereas that of empirical formula (14) fails to show the phenomenon. In addition, the energy dissipation rate of our model decays as k^{-3} (Figure 8a), which is closely to the field measurements by *Melville and Matusov* [2002] under a well-developed wave condition.

[20] The fractional energy dissipation can be defined as

$$(E_b - E_a)/E_b = \int_{k_1}^{k_2} (e_b(k) - e_a(k))dk \Big/ \int_{k_1}^{k_2} e_b(k)dk. \qquad (16)$$

Figure 9 shows the fractional energy dissipation $(E_b - E_a)/E_b$ due to breaking for a wind speed of 3 to 30 m s^{-1}. The fractional energy dissipation increases significantly as wind speed ranges from 3 to 20 m s^{-1}, but no significant increase is found at wind speed higher than 20 m s^{-1}. About 15% of the wave energy may be dissipated through breaking at wind speed up to 30 m s^{-1}.

4. Wave Momentum Loss by Wave Breaking

[21] Since wave energy and momentum densities are related by $m(k) = e(k)/c(k)$, the momentum density of surface waves in terms of the one-dimensional spectrum is

$$m_b(k) = \frac{1}{2}\rho_w g S(k)/c(k). \qquad (17)$$

Similarly, the momentum density after breaking can be expressed as

$$m_a(k) = \frac{1}{2}\rho_w g S_B(k)/c(k). \qquad (18)$$

Then, the distribution of wave momentum loss becomes

$$\varepsilon_{em}(k) = m_b(k) - m_a(k). \qquad (19)$$

[22] The empirical formula of momentum dissipation rate of breaking crest with respect to the wave phase speed is given by

$$\varepsilon_{Momentum} = b\rho_w g^{-1} c^4 \Lambda(c). \qquad (20)$$

In order to compare our model results with those of empirical formula (20), we use two proportional coefficients 0.0085 and 0.0007. Figure 10 shows that, at wind speed of 15 m s^{-1}, the momentum dissipation rate of our model lies between those estimated by empirical formula with proportional coefficients 0.0085 and 0.0007. In comparing Figures 11a and 11b, on the other hand, we find that though the peak momentum dissipation rate of our model is nearly

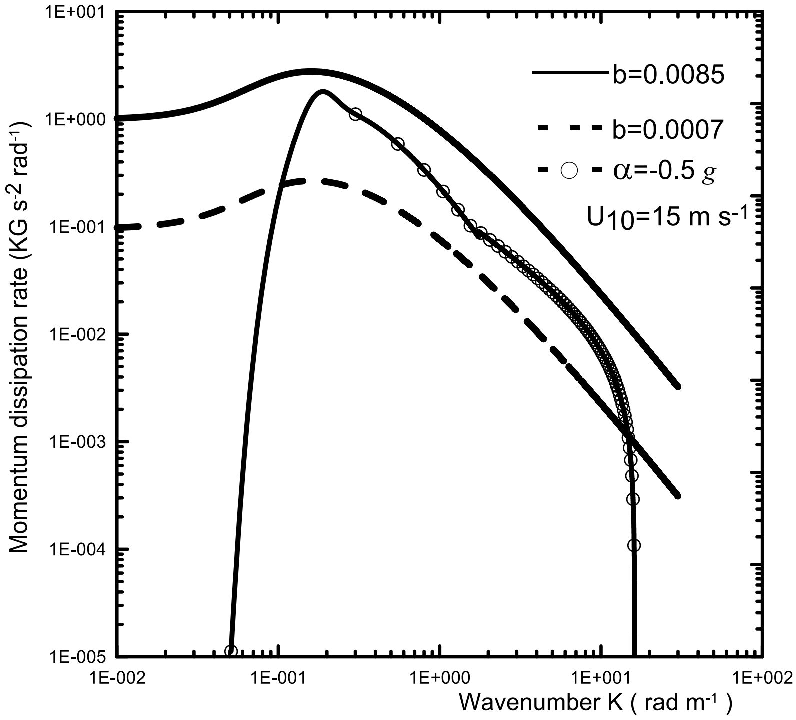

Figure 10. A comparison of momentum dissipation rates between our model and those estimated by empirical formula. Open circle is for our model result, solid line is for empirical results with a proportional coefficient of 0.0085 suggested by *Melville and Matusov* [2002], and dashed line is for empirical results with a proportional coefficient of 0.0007 reported by *Phillips et al.* [2001].

the same in magnitude as that estimated by empirical formula with a proportional coefficient of 0.006 at wind speed of 10, 15, and 20 m s^{-1}, respectively, the peak frequency of our model downshifts to the lower-frequency band as wind speed increases, whereas that of empirical formula (20) fails to show the phenomenon. In addition, the momentum dissipation rate of our model decays as $k^{-2.5}$, which is close to the field measurements of *Melville and Matusov* [2002] under a well-developed wave condition.

[23] The fractional momentum dissipation can be defined as

$$(M_b - M_a)/M_b = \int_{k_1}^{k_2} (m_b(k) - m_a(k))dk / \int_{k_1}^{k_2} m_b(k)dk. \quad (21)$$

The fractional momentum dissipation estimated by our model as a function of wind speed is shown in Figure 12. Figure 12 shows that the fractional momentum dissipation increases as wind speed ranges from 3 to 30 m s^{-1}. About 15% of the wave energy may be dissipated through breaking as wind speed up to 30 m s^{-1}.

5. Conclusions

[24] It is a formidable task to provide a detailed description of wave breaking and how it affects air-sea energy and momentum transfer. Although, strictly speaking, our model is only an approximate description of wave breaking, we believe that it captures the main features of wave breaking, which is important in determining the wave field dissipation.

[25] We have shown that the breaking wave coverage per unit time increases from 0.05 to 0.27 s^{-1} as wind speed ranges from 3.0 to 30 m s^{-1}, and the volume of breaking water per unit time and per unit area of wave surface increases significantly from 0.0 to 0.22 m s^{-1}, as wind speed ranges from 5.0 to 30 m s^{-1}under developing wave conditions.

[26] Breaking is believed to be the main factor in wave energy dissipation. We have concluded that the energy loss is mainly due to wave components at frequencies higher than the peak frequency. Though energy loss due to wave components at frequencies lower than the peak frequency is found, these wave components do not significantly lose energy after breaking. The energy dissipation rate, when expressed as phase speed c_b of breaking waves, is mainly in the range 0.20 $c_p < c_b <$ 0.90 c_p. In addition, the total energy loss is approximately proportional to the cube of wind speed in moderate and high sea states.

[27] Our work has also demonstrated that the energy and momentum dissipation rates decay like k^{-3} and $k^{-2.5}$, respectively. The fractional energy (or momentum) loss is not more than 15% for wind speed ranges from 3 to 30 m s^{-1} under developing wave conditions. Compared with the energy (or momentum) dissipation rate of empirical formula by wave breaking, our model result lies between those estimated by empirical formula with proportional coefficients 0.0085 and 0.0007. Furthermore, the peak frequency of our model energy (or momentum) dissipation rate downshifts to the lower-frequency band as the wind speed increases, whereas that of the empirical formula remains at the same frequency.

[28] It should be emphasized that the open sea observation of breaking rate is one field in which the presence of small-scale breakers is largely ignored. Further observation of breaking rate should include the contribution of small-

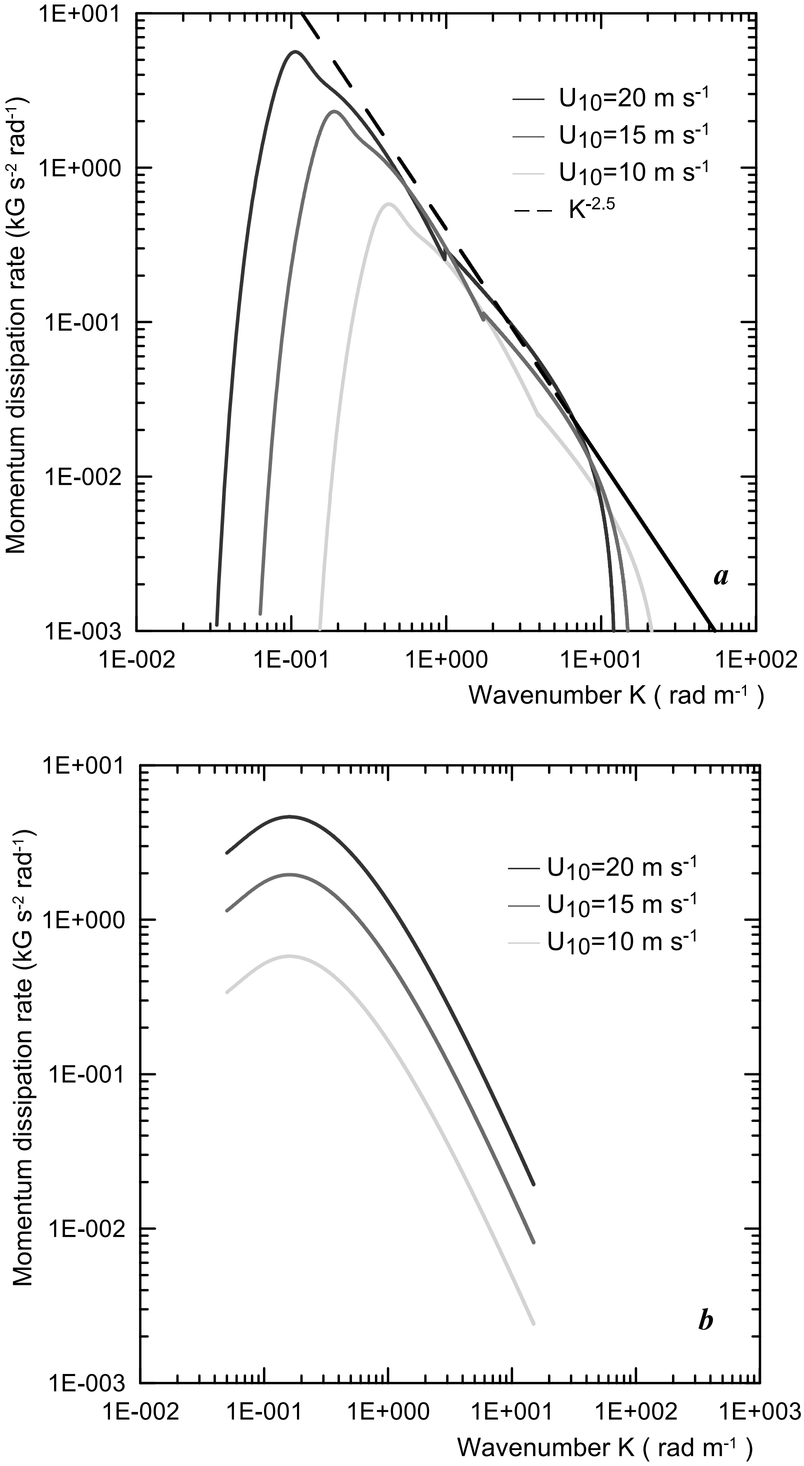

Figure 11. Momentum dissipation rates estimated for wind speeds of 10, 15 and 20 m s^{-1}. (a) Model results. (b) Estimated by empirical formula with the proportional coefficient of 0.006. See color version of this figure in the HTML.

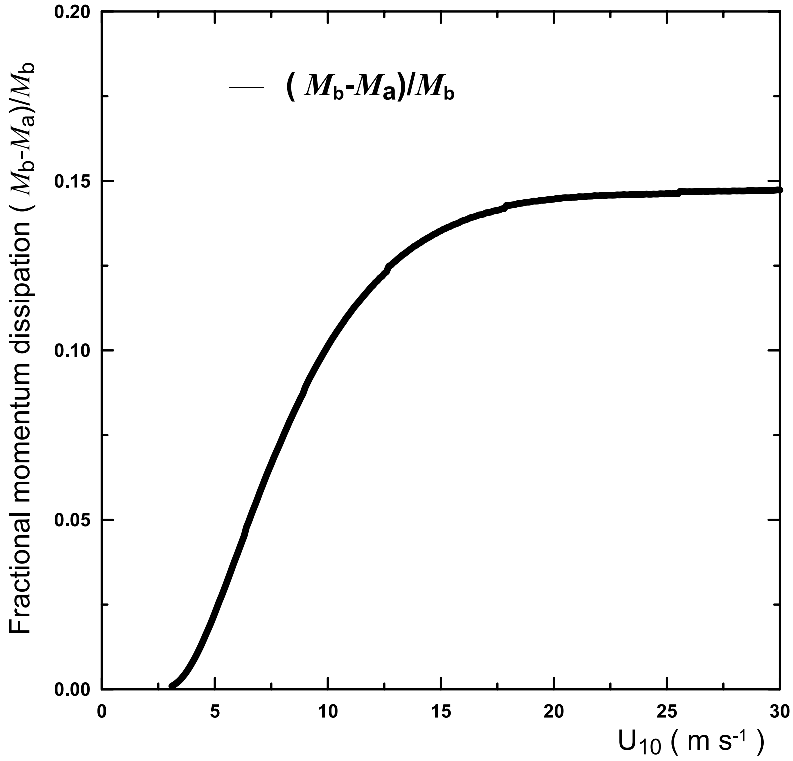

Figure 12. Fractional momentum dissipation versus wind speed of U_{10}. Solid line indicates our model results.

scale breakers, which may make an important contribution to breaking rate. Thermal imagery, rather than visible imagery, is likely to be important for resolving the statistics of capillary-gravity wave breaking [*Jessup et al.*, 1997; *Zappa et al.*, 2001].

[29] It should also be emphasized that the effects of the nonlinearity of sea waves and directional properties of wave breaking have not been considered in the present model. Both extensive study of the nonlinearity of wave field, especially the departure of wave height from a Gaussian distribution, and extending our model results to address directional properties of breaking waves to acquire a better estimate of total wave field dissipation by breaking is required.

Appendix A

[30] As in the same approach used by *Cartwright and Longuet-Higgins* [1956], *Yuan et al.* [1990] obtained the joint distribution of $(\zeta, \ddot{\zeta})$ per unit time in a normal original wave field $\{\zeta, p(\zeta, \dot{\zeta}, \ldots)\}$ under the condition of $\partial\zeta/\partial t$ (hereinafter $\dot{\zeta}$) to be a constant; this leads to

$$p(\zeta, \ddot{\zeta}|\dot{\zeta} = r) = \frac{p(\zeta, \dot{\zeta} = r, \ddot{\zeta})|\dot{\zeta}|}{\int_{-\infty}^{\infty}\int_{-\infty}^{\infty} p(\zeta, \dot{\zeta} = r, \ddot{\zeta})|\dot{\zeta}|d\zeta d\ddot{\zeta}}. \tag{A1}$$

The occurrence rate of $\dot{\zeta} = r$, that is, $N(r)$, can be expressed as

$$N(r) = \int_{-\infty}^{\infty}\int_{-\infty}^{\infty} p(\zeta, \dot{\zeta} = r, \ddot{\zeta})|\dot{\zeta}|d\zeta d\ddot{\zeta} \tag{A2}$$

Consequently, the joint distribution of $(\zeta, \ddot{\zeta})$ per unit time becomes [*Yuan et al.*, 1990]

$$\begin{aligned} p(\zeta, \ddot{\zeta}) &= \int_{-\infty}^{\infty} p(\zeta, \ddot{\zeta}|\dot{\zeta} = r)N(r)p(N)dN \\ &= \frac{|\ddot{\zeta}|}{4\pi^{3/2}(\mu_0\mu_2\mu_4)^{1/2}(1-\rho^2)^{1/2}} \\ &\quad \cdot \exp\left\{-\frac{1}{2(1-\rho^2)}\left[\left(\frac{\zeta}{\sqrt{\mu_0}}\right)^2 + 2\rho\frac{\zeta\ddot{\zeta}}{\sqrt{\mu_0\mu_4}} + \left(\frac{\ddot{\zeta}}{\sqrt{\mu_4}}\right)^2\right]\right\}, \end{aligned} \tag{A3}$$

where $\rho = \mu_2/(\mu_0\mu_4)^{1/2}$, μ_i is the ith-order moment of the wave spectrum. We assume that the wave fields are homogeneous and stationary. The breaking wave coverage per unit time can then be calculated by applying (A3) to equation (8) as

$$\begin{aligned} \Phi_B &= E\left\{H\left(-\frac{g}{2} - \ddot{\zeta}\right)\right\} \\ &= \frac{1}{4\pi^{3/2}(\mu_0\mu_2\mu_4)^{1/2}(1-\rho^2)^{1/2}} \\ &\quad \cdot \int_{-\infty}^{-g/2} |\ddot{\zeta}| \exp\left\{-\frac{1}{2}\left(\frac{\ddot{\zeta}}{\sqrt{\mu_4}}\right)^2\right\} d\ddot{\zeta} \\ &\quad \cdot \int_0^{\infty} \exp\left\{-\frac{1}{2(1-\rho^2)}\left(\frac{\zeta}{\sqrt{\mu_0}} + \rho\frac{\ddot{\zeta}}{\sqrt{\mu_4}}\right)^2\Bigg]\right\} d\zeta \end{aligned}$$

$$= \frac{1}{4\pi}\left(\frac{\mu_4}{\mu_2}\right)^{1/2}\frac{1}{2\pi^{1/2}}\int_{-\infty}^{\infty}\exp\left(-\frac{x^2}{2}\right)dx$$

$$\cdot \int_{g/2\mu_4^{1/2}}^{\infty} y\exp\left(-\frac{y^2}{2}\right)dy$$

$$= \frac{1}{4\sqrt{2}\pi}\left(\frac{\mu_4}{\mu_2}\right)^{1/2}\exp\left(-\frac{g^2}{8\mu_4}\right). \tag{A4}$$

Similarly, the volume of breaking water can be calculated as

$$V_B \approx \frac{\mu_0^{1/2}\mu_4^{3/2}}{2\pi^{3/2}g^2\mu_2^{1/2}}\exp\left(-\frac{g^2}{8\mu_4}\right). \tag{A5}$$

[31] **Acknowledgments.** We are grateful to reviewers for their helpful suggestions and comments on the manuscript and to Steve Thorpe for his editorial comments. The research presented in this paper is supported under the National 863 program of China (grant 2002AA633100).

References

Agrawal, Y. C., E. A. Terray, M. A. Donelan, P. A. Hwang, A. J. Williams III, W. M. Drennan, K. K. Kahma, and S. A. Kitaigorodskii (1992), Enhanced dissipation of kinetic energy beneath surface waves, *Nature*, *359*, 219–220.

Banner, M. L., and O. M. Phillips (1974), On the incipient breaking of small scale waves, *J. Fluid Mech.*, *65*, 647–656.

Cartwright, D. E., and M. S. Longuet-Higgins (1956), The statistical distribution of the maxima of a random function, *Proc. R. Soc. London, Ser. A*, *237*, 212–232.

Cox, C. S., and W. H. Munk (1954), Statistics of the sea surface derived from Sun glitter, *J. Mar. Res.*, *13*, 198–227.

Csanady, G. T. (1990), The role of breaking wavelets in air-sea gas transfer, *J. Geophys. Res.*, *95*, 749–759.

Dawson, T. H., D. L. Kriebel, and L. A. Wallendorf (1993), Breaking waves in laboratory-generated JONSWAP seas, *Appl. Ocean Res.*, *13*, 85–93.

Deane, G. B., and M. D. Stokes (2002), Scale dependence of bubble creation mechanisms in breaking waves, *Nature*, *418*, 839–844.

Ding, L., and D. M. Farmer (1994), Observations of breaking surface wave statistics, *J. Phys. Oceanogr.*, *24*, 1368–1387.

Duncan, J. H. (1981), An experimental investigation of breaking waves produced by a towed hydrofoil, *Proc. R. Soc. London, Ser. A*, *377*, 331–348.

Elfouhaily, T., B. Chapron, K. Katsaros, and D. Vandemark (1997), A unified directional spectrum for long and short wind-driven waves, *J. Geophys. Res.*, *102*, 15,781–15,796.

Erickson, D. J., III, C. Seuzaret, W. C. Keene, and S. L. Gong (1999), A general circulation model based on calculation of HCl and ClNO2 production from sea salt dechlorination: Reactive Chlorine Emissions Inventory, *J. Geophys. Res.*, *104*, 8347–8372.

Farmer, D. M., and J. R. Gemmrich (1996), Measurements of temperature fluctuations in breaking surface waves, *J. Phys. Oceanogr.*, *26*, 816–825.

Gemmrich, J. R., and D. M. Farmer (1999), Observations of the scale and occurrence of breaking surface waves, *J. Phys. Oceanogr.*, *29*, 2595–2606.

Gemmrich, J. R., T. D. Mudge, and V. D. Polonchicko (1994), On the energy input from wind to surface waves, *J. Phys. Oceanogr.*, *24*, 2413–2417.

Graham, A. (2004), Aeration due to breaking waves. Part II: Fluxes, *J. Phys. Oceanogr.*, *34*, 1008–1018.

Graham, A., D. K. Woolf, and A. J. Hall (2004), Aeration due to breaking waves. Part I: Bubble population, *J. Phys. Oceanogr.*, *34*, 989–1007.

Hara, T., E. J. Bock, and D. Lyzenga (1994), In situ measurements of capillary-gravity wave spectra using a scanning laser slope gauge and microwave radars, *J. Geophys. Res.*, *99*, 12,593–12,602.

Holthuijsen, L. H., and T. H. C. Herbers (1986), Statistics of breaking waves observed as whitecaps in the open sea, *J. Phys. Oceanogr.*, *16*, 290–297.

Hua, F., and Y. L. Yuan (1991), Breaking waves spectrum and its application, in *Breaking Waves*, edited by M. L. Banner and R. H. J. Grimshaw, pp. 277–282, Springer, New York.

Jähne, B., and K. S. Riemer (1990), Two-dimensional wave number spectra of small-scale water surface waves, *J. Geophys. Res.*, *95*, 11,531–11,546.

Jessup, A. T., C. J. Zappa, M. R. Loewen, and V. Hesany (1997), Infrared remote sensing of breaking waves, *Nature*, *385*, 52–55.

Kinsman, B. (1965), *Wind Waves: Their Generation and Propagation on the Ocean Surface*, Prentice-Hall, Upper Saddle River, N. J.

Kitaigorodskii, S. A. (1992), The dissipation subrange of wind-wave spectra, in *Breaking Waves*, edited by M. L. Banner and R. H. J. Grimshaw, pp. 200–206, Springer, New York.

Kway, J. H., Y. Loh, and E. Chan (1998), Laboratory study of deep-water breaking waves, *J. Ocean Eng.*, *25*, 657–676.

Lamarre, E., and W. K. Melville (1991), Air entrainment and dissipation in breaking waves, *Nature*, *351*, 469–472.

Lamarre, E., and W. K. Melville (1992), Instrumentation for the measurement of void-fraction in breaking waves: Laboratory and field results, *IEEE.J. Oceanic Eng.*, *17*, 204–215.

Longuet-Higgins, M. S. (1963), The generation of capillary waves by steep gravity waves, *J. Fluid Mech.*, *16*, 138–159.

Lou, S. L. (1997), Wave breaking in deep water, Ph.D. thesis, pp. 67–72, Inst. of Oceanol., Chin. Acad. of Sci., Qingdao, China.

Melville, W. K. (1994), Energy dissipation by breaking waves, *J. Phys. Oceanogr.*, *24*, 2041–2049.

Melville, W. K. (1996), The role of surface wave breaking in air-sea interaction, *Annu. Rev. Fluid Mech.*, *28*, 279–321.

Melville, W. K., and P. Matusov (2002), Distribution of breaking waves at the ocean surface, *Nature*, *417*, 58–63.

Melville, W. K., and R. J. Rapp (1985), Momentum flux in breaking waves, *Nature*, *317*, 514–516.

Meza, E., J. Zhang, and R. J. Seymour (2000), Free-wave energy dissipation in experimental breaking waves, *J. Phys. Oceanogr.*, *30*, 2404–2418.

Mitsuyasu, H. (1985), A note on the momentum transfer from wind to waves, *J. Geophys. Res.*, *90*, 3343–3345.

Monahan, E. C., and M. C. Spillane (1984), The role of oceanic whitecaps in air-sea gas exchange, in *Gas Transfer at Water Surfaces*, edited by W. Brutsaert, pp. 495–503, Springer, New York.

Nepf, H. M., C. H. Wu, and E. S. Chan (1998), A comparison of two- and three-dimensional wave breaking, *J. Phys. Oceanogr.*, *28*, 1496–1510.

Phillips, O. M. (1985), Statistical and spectral properties of the equilibrium range of wind-generated gravity waves, *J. Fluid Mech.*, *156*, 505–531.

Phillips, O. M., F. L. Posner, and J. P. Hansen (2001), High range resolution radar measurements of the speed distribution of breaking events in wind-generated ocean waves: Surface impulse and wave energy dissipation rates, *J. Phys. Oceanogr.*, *31*, 450–460.

Rapp, R. J., and W. K. Melville (1990), Laboratory measurements of deep-water breaking waves, *Philos. Trans. R. Soc. London, Ser. A*, *331*, 735–800.

Shaw, J. M. (2003), A microscopic view of oil slick break-up and emulsion formation in breaking waves, *Spill Sci. Technol. Bull.*, *8*, 491–501.

Smith, M. J., E. M. Poulter, and J. A. McGregor (1996), Doppler radar measurements of wave groups and breaking waves, *J. Geophys. Res.*, *101*, 14,269–14,282.

Snyder, R., L. Smith, and R. Kennedy (1983), On the formation of whitecaps by a threshold mechanism. Part III: Field experiment and comparison with theory, *J. Phys. Oceanogr.*, *13*, 1505–1518.

Terray, E. A., M. A. Donelan, Y. C. Agrawal, W. M. Drennan, K. K. Kahma, A. J. Williams III, P. A. Hwang, and S. A. Kitaigorodskii (1996), Estimates of kinetic energy dissipation under breaking waves, *J. Phys. Oceanogr.*, *26*, 792–807.

Thorpe, S. A. (1992), Bubble clouds and the dynamics of the upper ocean, *Q. J. R. Meteorol. Soc.*, *118*, 1–22.

Thorpe, S. A. (1993), Energy loss by breaking waves, *J. Phys. Oceanogr.*, *23*, 2498–2502.

Thorpe, S. A. (1995), Dynamical processes of transfer at the sea surface, *Prog. Oceanogr.*, *35*, 315–352.

Wang, W., and R. X. Huang (2004a), Wind energy input to the surface waves, *J. Phys. Oceanogr.*, *34*, 1276–1280.

Wang, W., and R. X. Huang (2004b), Wind energy input to the Ekman layer, *J. Phys. Oceanogr.*, *34*, 1267–1275.

Wu, J. (1992), Individual characteristics of whitecaps and volumetric description of bubbles, *IEEE J. Oceanic Eng.*, *17*, 150–158.

Yuan, Y. L., F. Hua, and Z. D. Pan (1990), Statistics of breaking waves and its application to upper ocean dynamics, *Sci. China, Ser. B*, *33*(1), 98–110.

Zappa, C. J., W. E. Asher, and A. T. Jessup (2001), Microscale wave breaking and air-water gas transfer, *J. Geophys. Res.*, *106*, 9385–9391.

Zhang, S. W., and Y. L. Yuan (2004), Statistics of breaking waves and its applications to estimation of air-sea fluxes, *Sci. China, Ser. D*, *47*(1), 78–85.

Zakharoff, V. E. (1992), Inverse and direct cascade in the wind-driven and surface wave turbulence and wave breaking, in *Breaking Waves*, edited by M. L. Banner and R. Grimshaw, pp. 70–91, Springer, New York.

Y. Yuan and S. Zhang, Key Laboratory of Marine Science and Numerical Modeling, First Institute of Oceanography, SOA, Qingdao 266061, China. (zhangsw@fio.org.cn)